Effect of Water Density on Hydrogen Peroxide Dissociation in Supercritical Water. 1. Reaction Equilibrium

Naoko Akiya and Phillip E. Savage*

Department of Chemical Engineering, University of Michigan, Ann Arbor, Michigan 48109-2136

Received: June 23, 1999; In Final Form: December 3, 1999

Recent experiments showed that the rate of dissociation of H_2O_2 in supercritical water (SCW) is density dependent and faster than its high-pressure limit rate in the gas phase. These observations suggest that water molecules play a role in this reaction in SCW. We performed density functional theory (DFT) calculations and molecular dynamics simulations to investigate the role of water in H_2O_2 dissociation. We generated the potential energy surface for H_2O_2−water and OH−water complexes by DFT calculations to determine the parameters in an analytical intermolecular potential model, which was subsequently employed in the molecular dynamics simulations. These simulations were performed at different water densities. They provided the structural properties (pair correlation functions) of dilute mixtures of H_2O_2 and OH in SCW, from which we were able to calculate the number of excess solvent molecules and partial molar volumes for each solute. We used the partial molar volumes for H_2O_2 and OH to calculate the reaction volume for $H_2O_2 = 2OH$ and thereby determined the density dependence of the equilibrium constant for this reaction. The results show that at the reduced temperature of $T_r = 1.15$ (695 K) the equilibrium constant for H_2O_2 dissociation is a function of the water density. The mean value of the equilibrium constant changes by less than 5% between $0.25 < \rho_r < 1$, but it decreases by an order of magnitude between $1 < \rho_r < 2.75$. Knowing the density dependence of the equilibrium constant for this reaction will allow more accurate mechanism-based models of supercritical water oxidation chemistry to be developed. The computational approach applied herein for H_2O_2 dissociation is general and can be profitably employed to discern the density dependence of the equilibrium constant of any elementary reaction in SCW. There is currently no experimental approach that will provide this information for reactions involving free radicals.

1. Introduction

The oxidation of organic compounds in water above its critical temperature and pressure ($T > 374$ °C, $P > 218$ atm) has attracted intense interest, primarily as a waste treatment technology, but also as a means of chemical synthesis.[1,2] As a result of this interest, the oxidation rates of many organic compounds in supercritical water (SCW) have received scrutiny. Some of these investigations examined the effect of isothermal changes in the system pressure (and hence water density) on the reaction kinetics and found the rates to be pressure- (or density-) dependent. Interestingly, changes in the water density influence the oxidation rates differently for different compounds. For some compounds the rate increases with increasing density,[3−5] for others it decreases,[6−8] and for yet others the rate is independent of the water density.[9,10]

In this article we explore the influence of water density on the reaction equilibrium constant, and we use hydrogen peroxide dissociation ($H_2O_2 = 2OH$) in SCW as the model reaction. We will refer to water above its critical temperature as "supercritical" regardless of its pressure or density. We report results from a molecular dynamics simulation study of water density effects on the structural properties of dilute mixtures of hydrogen peroxide (H_2O_2) and hydroxyl radical (OH) in SCW. We then used these simulation results to determine the water density effects on the reaction equilibrium constant for $H_2O_2 = 2OH$. This study is a first step toward a better understanding of the water density effects on H_2O_2 dissociation and, ultimately, water density effects on supercritical water oxidation (SCWO).

* Corresponding author. E-mail: psavage@umich.edu.

1.1. Effect of Density on Equilibrium Constant.

The effect of pressure (P) on a reaction equilibrium constant (K_c), which is the ratio of forward and reverse rate constants (k_f /k_r), is expressed in terms of the reaction volume ($\Delta\bar{v}_{rxn}$):[11]

$$\left(\frac{\partial \ln K_c}{\partial P}\right)_T = -\frac{\Delta\bar{v}_{rxn}}{RT} + \kappa_T \sum \nu_i \qquad (1)$$

where $\sum\nu_i$ is the sum of the stoichiometric coefficients for the reaction, and κ_T is the isothermal compressibility. The reaction volume is defined as the sum of the products of the stoichiometric coefficient and the partial molar volume ($\bar{v}_i$) for each species in the reaction. In the case of H_2O_2 dissociation, the reaction volume is

$$\Delta\bar{v}_{rxn} = \sum \nu_i \bar{v}_i = 2\bar{v}_{OH} - \bar{v}_{H_2O_2} \qquad (2)$$

For a compressible fluid, isothermal changes in pressure cause changes in density. The effect of density ρ on the equilibrium constant is given by[2]

$$\left(\frac{\partial \ln K_c}{\partial \rho}\right)_T = \frac{1}{\rho\kappa_T}\left(\frac{\partial \ln K_c}{\partial \rho}\right)_T = \frac{1}{\rho}\left(-\frac{\Delta\bar{v}_{rxn}}{RT\kappa_T} + \sum \nu_i\right) \qquad (3)$$

Thus, the effect of density on an equilibrium constant can be easily characterized using the reaction volume, which can be determined from the partial molar volumes of reactants and products. The difficulty in using eqs 2 and 3 with experimental data is that experimental measurements of partial molar volumes are challenging.[12] For mixtures containing free radicals, this

10.1021/jp9920996 CCC: $19.00 © 2000 American Chemical Society
Published on Web 04/18/2000

difficulty is compounded by the low concentrations and short lifetimes of these highly reactive species. It is possible, however, to measure the equilibrium concentrations of molecular reactants and products using spectroscopic techniques and thereby directly determine equilibrium constants at various densities without using reaction volumes. This approach has been used to study density effects on reaction equilibria and kinetics in supercritical fluids.[12−15] This approach is suited for single-step reactions involving only molecular reactants and products. H_2O_2 dissociation, however, involves free-radical products (OH). There have been no reports of experimental measurements of free radical concentrations in SCW.

An alternative approach to experimental measurements of partial molar volumes or equilibrium constants is theoretical determination of these quantities. A formalism that is useful for this purpose is Kirkwood−Buff fluctuation theory.[16] This theory and its extension have been widely applied to describe dilute supercritical fluid mixtures.[17−21] In this formalism, the partial molar volume at infinite dilution ($\bar{v}_U^\infty$) can be calculated as

$$\rho\bar{v}_U^\infty = 1 - \rho(G_{UV} - G_{VV}) \tag{4}$$

where G_{UV} and G_{VV} are solute−solvent and solvent−solvent fluctuation integrals, respectively. The subscript U refers to the solute and V to the solvent. The superscript ∞ indicates the infinite dilution limit. These fluctuation integrals are a function of pair correlation functions ($g_{ij}(r)$):

$$G_{ij} = 4\pi\int_0^\infty [g_{ij}(r) - 1]r^2\,\mathrm{d}r \tag{5}$$

Thus, partial molar volumes depend on the relative strengths of the solute−solvent and solvent−solvent interactions. Pair correlation functions can be calculated directly from molecular simulations or integral equation methods. Therefore, partial molar volumes are easily determined from theory.

1.2. Significance of H_2O_2 Dissociation. Dissociation of H_2O_2 into highly reactive OH radicals is one of many elementary reaction steps that comprise the overall reaction mechanism of SCWO. This reaction is of great importance in the global SCWO kinetics. Sensitivity analyses performed on mechanism-based kinetics models for SCWO show that calculated reactant conversions and product yields are extremely sensitive to the kinetics of this single elementary step.[22−25] For instance, for methanol SCWO, a 10% change in the rate constant of H_2O_2 dissociation results in a 55% change in the predicted carbon dioxide concentration.[22] For SCWO of hydrogen, roughly two-thirds of the total uncertainty in the predicted hydrogen concentration comes from the uncertainty in the rate constant for H_2O_2 dissociation.[25]

In addition to its influence on global SCWO kinetics, H_2O_2 dissociation in SCW is also significant because its rate in SCW is faster than the gas-phase high-pressure limit rate.[26] Additionally, the authors of this experimental study stated that the global rate constant for H_2O_2 decomposition in SCW is pressure-independent, but their data clearly show that the rate constant is consistently lower at the higher pressure (see Figure 1). Thus, the kinetics of H_2O_2 dissociation in SCW are influenced by the water density.

Given the tremendous impact the kinetics of H_2O_2 dissociation has on the global SCWO kinetics and the experimentally observed density dependence of its kinetics, investigation of this reaction in SCW should elucidate some aspects of the water density effects on SCWO kinetics. An additional advantage for studying this reaction is that whatever insights we gain into the kinetics and equilibrium of H_2O_2 dissociation in SCW should help reduce the overall uncertainty in the mechanism-based models of SCWO kinetics.

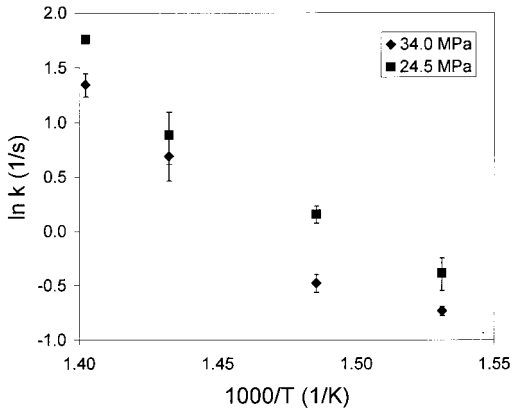

Figure 1. Experimental rate constants for H_2O_2 dissociation in supercritical water (ref 26).

2. Method

To conduct molecular dynamics simulations of dilute solutions of H_2O_2 and OH in SCW, one needs quantitative models for the H_2O_2−water, OH−water, and water−water intermolecular interactions. One may also include intramolecular forces, and we have chosen to do so.

2.1. Potential Model for Water. We used the flexible water model proposed by Teleman et al.,[27] which we refer to as the TJE model, to describe both the intermolecular and intramolecular potentials for water. This model is the rigid simple point charge (SPC) model[28] retrofitted with harmonic potentials that describe the intramolecular interactions. We selected a flexible model (one in which the O−H bond lengths and the H−O−H angle can be distorted) with the hope that by so doing we would capture the effects of the intramolecular dynamics of real water molecules, which of course are flexible. There are two reasons we selected the TJE model from among the different flexible models that have been developed for water. First, it is a simple model that is easily implemented. Second, the TJE model is the only flexible model that has been tested extensively for simulating SCW[29−34] and for which the critical point has been determined.[29]

The TJE model describes the interaction between water molecules as a sum of electrostatic and Lennard-Jones interactions:

$$V_{mn} = \sum_i^m\sum_n^j\left\{\frac{q_iq_j}{4\pi\epsilon_0 r_{ij}} + 4\epsilon_{ij}\left[\left(\frac{\sigma_{ij}}{r_{ij}}\right)^{12} - \left(\frac{\sigma_{ij}}{r_{ij}}\right)^{6}\right]\right\} \tag{6}$$

The indices i and j refer to atomic sites on molecules m and n, and r_{ij} is the distance between sites i and j. The parameters q_i and q_j are partial charges on atomic sites, and they account for electrostatic interactions. Only the oxygen atoms interact through the Lennard-Jones potential. Hydrogen atoms interact with each other and with oxygen atoms through the electrostatic potential. The intramolecular potential of a water molecule is described by a harmonic potential of the form:

$$V_i = \frac{k}{2}(x - x_e)^2 \tag{7}$$

In eq 7, x refers to an internal coordinate of a molecule, i.e., either a bond length or an angle, and x_e represents the

equilibrium geometry. The literature[27,28] provides numerical values for the partial charges (q_i) and Lennard-Jones parameters (σ_{ij}, ϵ_{ij}) in eq 6 as well as the equilibrium geometry and force constants (k) in eq 7.

2.2. Potential Model for H_2O_2−H_2O and OH−H_2O Interactions. The literature provides no potential model for the H_2O_2−water or OH−water interactions, so it was necessary to develop one for this study. This solute−water intermolecular potential model was obtained as an analytical function that was fit to the potential energy surface for the H_2O_2−water and OH−water dimers generated by density functional theory (DFT) calculations.

We used the following functional form to describe the solute−solvent intermolecular potential:

$$V_{mn} = \sum_{i}^{m}\sum_{n}^{j}\left\{\frac{q_i q_j}{4\pi\epsilon_0 r_{ij}} + \frac{A_{ij}}{r_{ij}^{12}} - \frac{B_{ij}}{r_{ij}^{6}}\right\} \qquad (8)$$

The indices i and j refer to atomic sites on molecules m and n, and r_{ij} is the distance between sites i and j. The partial charges for water were taken from the TJE model (section 2.1). The partial charges for H_2O_2 and OH were taken from the DFT calculations for isolated H_2O_2 and OH, respectively, using the method described below in section 2.2.1. The parameters A_{ij} and B_{ij} are adjustable, and their values were determined by fitting eq 8 to the DFT interaction energies, as described in the balance of this section.

2.2.1. DFT Calculations. We used density functional theory with the B3LYP functional[35−37] and the 6-311+G(3df,2p) basis set for all calculations. These choices were made because electron correlation must be taken into account[38] and a large, polarized basis set is necessary[38,39] to describe H_2O_2 adequately. Although second-order Møller−Plesset theory (MP2) sufficiently accounts for the electron correlation,[39] hybrid density functionals, which are computationally more efficient, can reproduce the MP2 and G2(MP2) results for H_2O_2 dimer and H_2O_2−water dimer, provided that large basis sets are used.[40] The B3LYP functional has been used previously for OH−water dimer.[41] We used Boys and Bernardi's counterpoise method[42] to correct for basis-set superposition error. We calculated the partial charges for each atom in H_2O_2 and OH using the CHelpG method.[43] This method finds the discrete partial atomic charges that best reproduce the quantum mechanical electrostatic potential of the molecule. *Gaussian94*, Revision B.3,[44] was used for all calculations.

2.2.2. Potential Energy Surface. To generate the potential energy surface for H_2O_2−water and OH−water dimers, we chose to sample energy-distributed geometries, or geometries that are representative of the relevant (low energy) portion of the potential energy surface. Our approach, which follows that of Jorgensen,[45] is outlined below.

The minimum energies of H_2O_2−water and OH−water dimers were determined by performing geometry optimization from various starting configurations. See Figure 2 and Table 1 for optimized geometries. The interaction energy was calculated by taking the difference between the dimer energy and monomer energies and accounting for the basis-set superposition error. See Table 2 for SCF energies of all optimized species. The resulting minimum interaction energy is −24.5 kJ/mol for H_2O_2−water and −19.4 kJ/mol for OH−water, so we randomly generated geometries for both dimers with (estimated) interaction energies ranging from −25 to 25 kJ/mol. We divided this energy range into 20 bins at 2.5 kJ/mol increments, and for each bin we accumulated 10 configurations of H_2O_2−water and OH−water dimer geometries. Thus, a total of 400 geometries were accumulated. The monomer geometries were fixed to the optimized values, and the dimer "bond" length and angles that define the intermolecular separation and orientation were generated by scaling random numbers[46] between 0 and 1. The length was scaled by 10 Å, which was the cutoff used to calculate the nonbonded forces in the molecular dynamics simulation. Angles were scaled by π, and dihedral angles were scaled by 2π.

For each dimer configuration that was generated, its interaction energy was estimated using a potential model of the form given in eq 8. The parameters A_{ij} and B_{ij} in eq 8 were approximated as $4\epsilon_{ij}\sigma_{ij}^{12}$ and $4\epsilon_{ij}\sigma_{ij}^{6}$, respectively, where ϵ_{ij} and σ_{ij} are Lennard-Jones parameters. The Lennard-Jones parameters for water were taken from the TJE model (section 2.1). The Lennard-Jones parameters for H_2O_2 and OH were taken from the values used in a previous molecular dynamics simulation of HO_2 in SCW.[30] We used the Lorentz−Berthelot combining rules for Lennard-Jones parameters of dissimilar atom types.

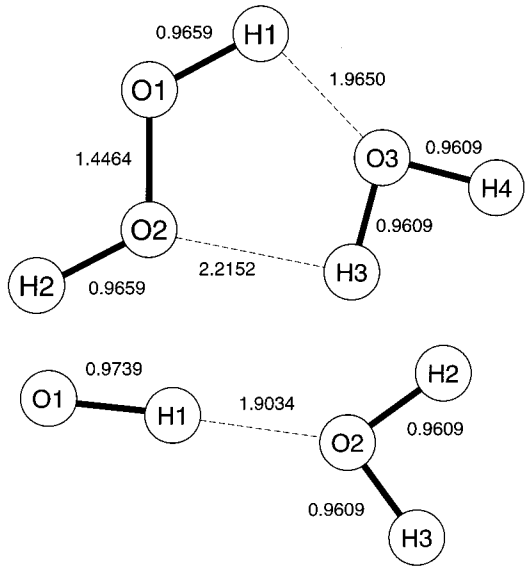

Figure 2. Optimized geometries for H_2O_2−water dimer and OH−water dimer. Distances shown are in ångstroms.

TABLE 1: Optimized Angles (degree) for H_2O_2−Water and OH−Water Dimers

H_2O_2−water		OH−water	
H3−O3−H4	105.1469	H2−O2−H3	105.1469
H1−O1−O2	100.8982	O1−H1−O2	179.9882
O1−O2−H2	100.8982	H1−O2−H2	127.4429
O1−H1−O3	144.7969	H1−O2−H3	127.4102
H1−O3−H3	80.5965	O1−H1−O2−H2	179.9952
H1−O3−H4	119.8135	O1−H1−O2−H3	0.0048
O3−H3−O2	123.6581		
H3−O2−O1	89.1180		
H1−O1−O2−H2	111.9324		
O1−H1−O3−H3	3.1682		
O1−H1−O3−H4	105.3114		
O2−O1−H1−O3	5.1740		
H1−O3−H3−O2	7.2050		

TABLE 2: SCF Energies for Optimized Structures

structure	SCF energy with BSSE correction (hartree)
H_2O_2	−151.612 199 866
H_2O	−76.464 104 480
H_2O_2−H_2O	−228.085 629 175
OH	−75.766 233 423
H_2O	−76.464 205 183
OH−H_2O	−152.237 820 522

TABLE 3: Parameters for the Solute−Water Potential Model

parameter	site pair	value
A_{ij} (kJ Å^{12}/mol)	$O_{H_2O_2}-O_{H_2O}$	3.58×10^5
	$O_{H_2O_2}-H_{H_2O}$	6.68×10^3
	$H_{H_2O_2}-O_{H_2O}$	1.03×10^4
	$H_{H_2O_2}-H_{H_2O}$	5.95×10^2
B_{ij} (kJ Å^6/mol)	$O_{H_2O_2}-O_{H_2O}$	-9.79×10^2
	$O_{H_2O_2}-H_{H_2O}$	0.00×10^0
	$H_{H_2O_2}-O_{H_2O}$	0.00×10^0
	$H_{H_2O_2}-H_{H_2O}$	2.19×10^1
q (elementary charge)	$O_{H_2O_2}$	−0.366
	$H_{H_2O_2}$	0.366
	O_{H_2O}	−0.81
	H_{H_2O}	0.42

This approximate potential model was used simply to assign the randomly generated dimers to the appropriate energy bin, and thereby provide an adequate number of energy-distributed dimers. DFT calculations were subsequently performed on all the dimers to determine the potential energy surfaces for H_2O_2−water and OH−water interactions.

2.2.3. Parameters for the Intermolecular Potential. After obtaining the DFT interaction energies for the 400 energy-distributed H_2O_2−water and OH−water dimers, we next used these energies to determine the parameters A_{ij} and B_{ij} in eq 8. As mentioned above, the partial charges were taken from the DFT/CHelpG calculations (H_2O_2, OH) and the TJE model (water).

We used a weighted nonlinear regression routine to fit eq 8 to the DFT interaction energies of the various configurations of both H_2O_2−water and OH−water dimers. Separate data fitting for H_2O_2−water and OH−water dimers did not produce a better fit. We used the following weighting function, which is designed to enhance the fit of low-energy data points:

$$w_i = 1 + \alpha \exp\left(-\frac{\Delta E_i - \Delta E_0}{RT}\right) \tag{9}$$

where α is an adjustable parameter, ΔE_i is the interaction energy of dimer i, and ΔE_0 is the reference interaction energy, chosen to be approximately that of the minimum energy dimer. We chose $\Delta E_0 = -25$ kJ/mol for H_2O_2 data and -20 kJ/mol for OH data. Following the examples of Jorgensen[45] and Swaminathan et al.,[47] we used $\alpha = 100$. We chose $T = 700$ K, which is a representative temperature for experimental studies of SCWO.

The optimal values of the parameters A_{ij} and B_{ij} and the partial charges are given in Table 3. We emphasize that the values of these parameters are simply those that produced the best fit and that one should not attach any physical meaning to them. Figure 3 shows a parity plot that compares the interaction energies for H_2O_2−water and OH−water dimers obtained from the DFT calculations and those calculated from eq 8 with parameters given in Table 3.

2.3. Intramolecular Potential Model for H_2O_2 and OH. The intramolecular dynamics of an H_2O_2 molecule were described by the potential model of Getino et al.[48,49] This model assumes that the potential is separable in internal coordinates:

$$V = V_{\text{stretch}} + V_{\text{bend}} + V_{\text{tors}} \tag{10}$$

The first term is a sum of Morse functions describing bond stretching:

$$V_{\text{stretch}} = \sum_{i=1}^{3} D_i\{1 - \exp[-\beta_i(r_i - r_i^0)]\}^2 \tag{11}$$

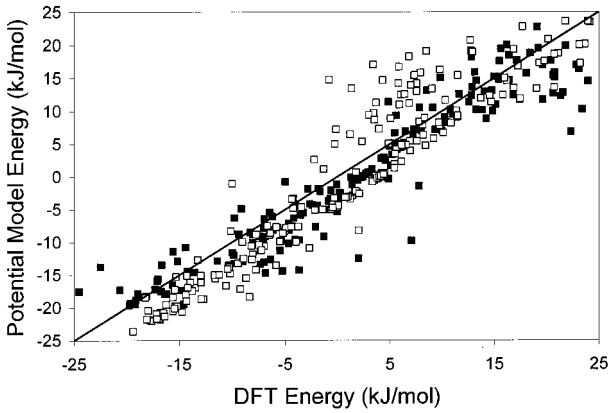

Figure 3. Parity plot for (■) H_2O_2−water and (□) OH−water interaction energies calculated from the potential model (eq 8) and from DFT calculations.

where r_i and r_i^0 are the length of bond i and its equilibrium value, respectively. Parameters D_i and β_i are empirical constants for bond i. The second term is a sum of harmonic potentials that describe angle bending:

$$V_{\text{bend}} = 0.5\sum_{j=1}^{2} S(r_{\text{OO}})S(r_{\text{OH}})K_j(\Theta_j - \Theta_j^0) \tag{12}$$

where Θ_j and Θ_j^0 are the magnitude of angle j and its equilibrium value, respectively. K_j is the force constant of angle j. The third term is the torsional potential described by a four-term Fourier series:

$$V_{\text{tors}} = S(r_{\text{OO}})\sum_{n=0}^{3} A_n \cos(n\varphi) \tag{13}$$

where φ is the dihedral angle. The switching functions $S(r_{\text{OO}})$ and $S(r_{\text{OH}})$ are used to attenuate the force constants K_j and A_n as H_2O_2 dissociates. We used the Morse potential (eq 11) with O−H bond parameters to describe the intramolecular dynamics of an OH radical.

2.4. Molecular Dynamics Simulation Procedure. All simulations were conducted in a canonical ensemble (*NVT*), which comprised a single H_2O_2 or OH in a simulation box with 499 water molecules (i.e., mole fraction = 0.002) to approximate infinitely dilute mixtures. We used a reduced temperature of $T_r = 1.15$ and reduced densities of $\rho_r = 0.25$, 0.33, 0.42, 0.50, 0.75, 0.88, 1.12, 1.25, 1.75, 2.25, and 2.75. The critical properties of TJE water were used to calculate these reduced properties. The critical point for TJE water is $T_c = 604.3$ K and $\rho_c = 269.4$ kg/m^3 [29] whereas the critical point of real water is $T_c = 647.1$ K and $\rho_c = 322.0$ kg/m^3.

We used the reversible reference system propagator algorithm (r-RESPA)[50,51] to handle the dynamics that evolve at different time scales. We took the long time step to be 1 fs and the short time step to be 0.1 fs for all simulations. The Nosé−Hoover method[52,53] was used for temperature control to ensure that a canonical ensemble was obtained. The method was implemented with a single thermostat with a fluctuation period of 10 fs. For each simulation, we equilibrated the system for at least 400 ps and accumulated data for 1.8 ns.

Standard simulation procedures including the Verlet neighbor list, periodic boundary conditions, and the minimum image convention were used.[54,55] All interactions were truncated at 10 Å. The long-range electrostatic interactions were treated with the reaction field method.[54,56] The dielectric constant of the

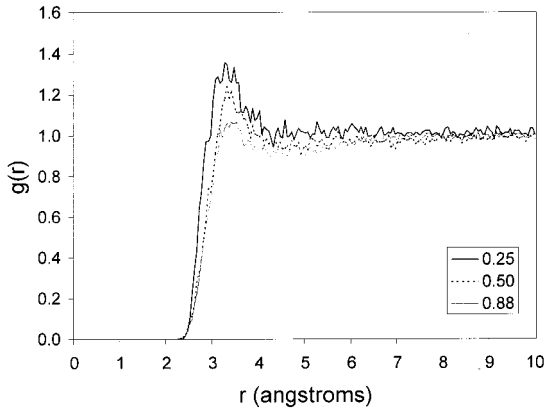

Figure 4. H_2O_2−water pair correlation functions at $T_r = 1.15$ and $\rho_r = 0.25$, 0.50, and 0.88.

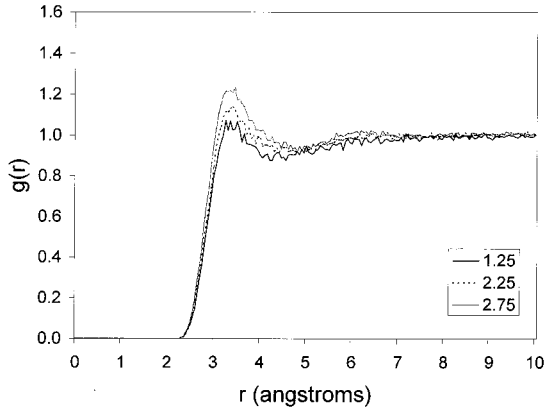

Figure 5. H_2O_2−water pair correlation functions at $T_r = 1.15$ and $\rho_r = 1.25$, 2.25, and 2.75.

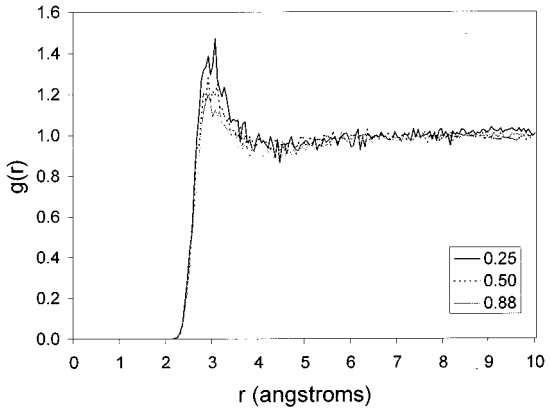

Figure 6. OH−water pair correlation functions at $T_r = 1.15$ and $\rho_r = 0.25$, 0.50, and 0.88.

dielectric continuum, ϵ^{RF} was chosen to be 80, as any value of ϵ^{RF} between the value of the true dielectric constant and infinity is acceptable for moderately and highly polar substances.[56] The dielectric constant of SCW is lower than that of ambient water, which is about 80.

3. Results and Discussion

3.1. Structural Properties. Figures 4−7 show the solute−solvent pair correlation functions for H_2O_2−water and OH−water pairs. The correlations were determined using center-of-mass separations. We sampled pair correlation functions every 50 fs using a sampling bin width of 0.5 Å. The choppy appearance of the solute−water pair correlation functions in

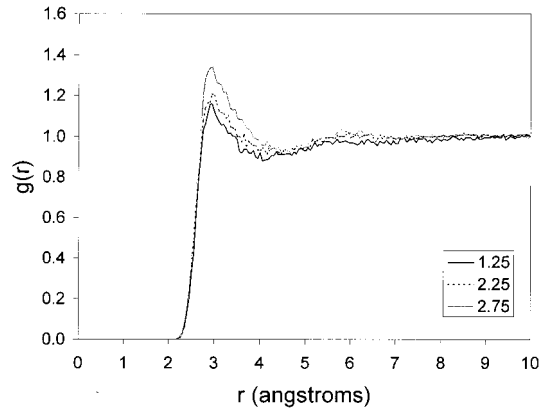

Figure 7. OH−water pair correlation functions at $T_r = 1.15$ and $\rho_r = 1.25$, 2.25, and 2.75.

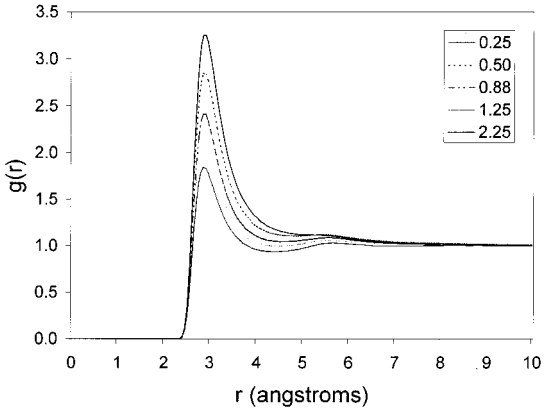

Figure 8. Water−water pair correlation functions at $T_r = 1.15$ and $\rho_r = 0.25$, 0.50, 0.88, 1.25, and 2.25.

Figures 4−7 is also apparent in results from other molecular dynamics studies of dilute supercritical mixtures.[19,57−59] The correlations for subcritical and supercritical solvent densities are shown separately for clarity. These figures show that the pair correlation functions exhibit different density dependences at subcritical and supercritical densities. Below the critical density of water, the peak height decreases with increasing density. On the other hand, above the critical density, the peak height increases with increasing density. Figure 8 shows the corresponding water−water pair correlation functions obtained from simulations for both H_2O_2−water and OH−water mixtures. In contrast to the solute−water correlation functions, the water−water correlation functions show a monotonic decrease in peak height with increasing water density. These contrasting trends for solute−water and water−water correlations suggest that the strengths of solute−water interactions relative to water−water interactions may be sensitive to changes in the water density.

To better understand the interplay between solute−water and water−water interactions at different water densities, we calculated the number of excess solvent molecules (N^{ex}), defined as[19]

$$N^{ex} = \rho(G_{UV} - G_{VV}) \tag{14}$$

where G_{UV} and G_{VV} are calculated from eq 5. The integration in eq 5 was carried out to $r = 10$ Å. N^{ex} was calculated at each 200 ps interval during the simulation. Since we had multiple determinations of N^{ex} at each state point, we were able to calculate the mean and the standard deviation of N^{ex} for each state point. The definition in eq 14 gives the number of solvent

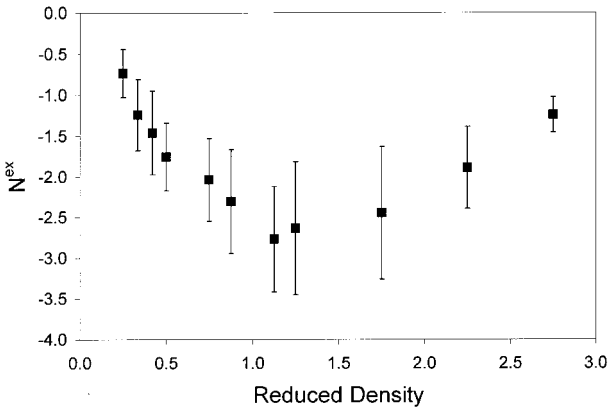

Figure 9. Number of excess solvent molecules for H_2O_2 in water at $T_r = 1.15$.

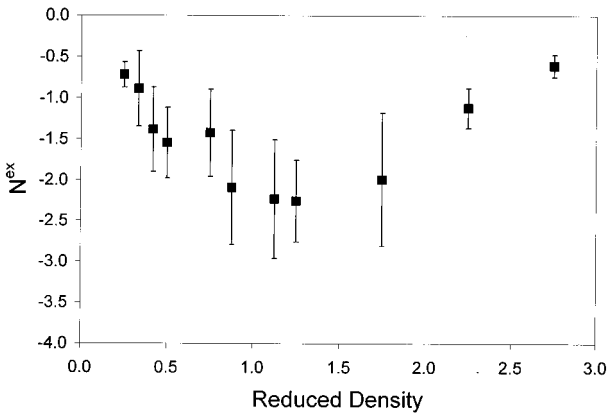

Figure 10. Number of excess solvent molecules for OH in water at $T_r = 1.15$.

molecules around the solute molecule in excess of the number that would be there if the solute molecule were simply another solvent molecule. This definition differs slightly from a more common one for the number of excess solvent molecules, $n^{ex} = \rho G_{UV}$.[20,60] We use eq 14, however, because it measures the extent of perturbation of the solvent structure due to the presence of the solute. Figures 9 and 10 show the number of excess water molecules (from eq 14) around H_2O_2 and OH at different densities. The negative sign of N^{ex} indicates that there is a depletion of water molecules around H_2O_2 and OH compared to that around another water molecule. Thus, solute−water interactions are less attractive than water−water interactions. For both H_2O_2 and OH, the magnitude of N^{ex} or the extent of water depletion around the solute appears to go through a maximum near $\rho_r \approx 1$.

The number of excess solvent molecules as defined by eq 14 is related to the solute partial molar volume at infinite dilution, $\bar{v}_U^\infty$. Combining eqs 4 and 14, we obtain

$$\bar{v}_U^\infty = \frac{1 - N^{ex}}{\rho} \tag{15}$$

Figures 11 and 12 show the solute partial molar volumes for H_2O_2 and OH in water at $T_r = 1.15$ and different water densities as calculated from eq 15. We determined the uncertainties for all the partial molar volumes and other calculated properties that we report in this paper from the uncertainty for N^{ex} and the propagation of errors formula. The partial molar volume decreases with increasing water density for both H_2O_2 and OH at this temperature. This density dependence is somewhat expected, since the partial molar volume is inversely proportional to the solvent density and directly proportional to the solvent isothermal compressibility:[20,61]

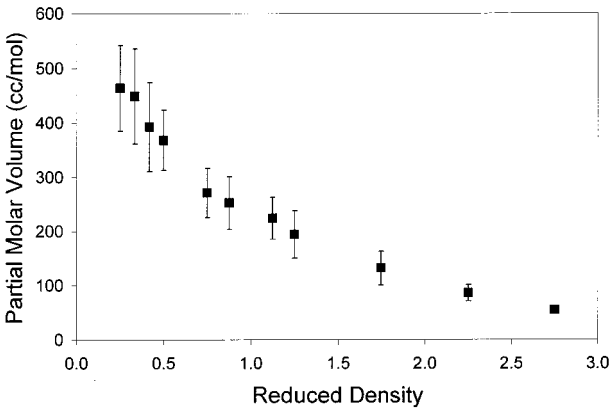

Figure 11. H_2O_2 partial molar volumes in SCW at $T_r = 1.15$.

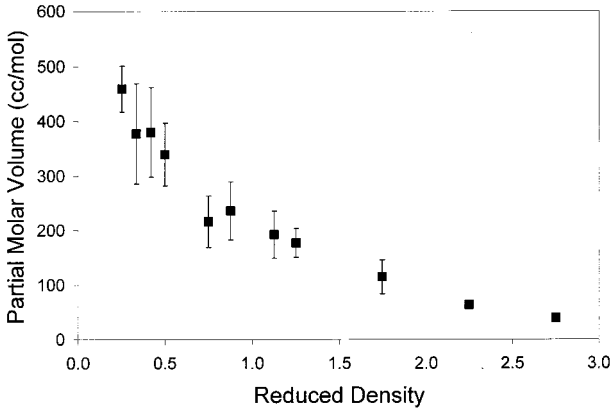

Figure 12. OH partial molar volumes in SCW at $T_r = 1.15$.

$$\bar{v}_U^\infty = \frac{\kappa_T}{\rho}(1 - x_U)\left(\frac{\partial P}{\partial x_U}\right)_{T,V} \tag{16}$$

where x_U is solute mole fraction. At $T_r = 1.15$, κ_T decreases monotonically with density. Also, note the magnitude of the partial molar volume. A typical value for liquid mixtures is on the order of 10 cm^3/mol. At the temperature and densities that we studied, the partial molar volume is an order of magnitude higher, reflecting the compressible nature of supercritical water. The positive sign of $\bar{v}_U^\infty$ means that solute−water interactions are less attractive than water−water interactions and hence the addition of a solute to the mixture results in an increase in the mixture volume. Negative N^{ex} and positive $\bar{v}_U^\infty$ suggest that dilute mixtures of H_2O_2 in water and OH in water are "repulsive," according to the classification by Debenedetti.[20,60]

3.2. Density Effects on Reaction Equilibrium. In this section we use the mixture properties that we have calculated to gain some insight into the reaction equilibrium constant for H_2O_2 dissociation in SCW. Since we have determined the partial molar volumes of H_2O_2 and OH in SCW, we can calculate the reaction volume for $H_2O_2 = 2OH$ in SCW and thereby elucidate the water density effects on the equilibrium constant from eq 3. Figure 13 shows the reaction volume calculated for H_2O_2 dissociation at different water densities. The reaction volume has the same water-density dependence and the same order of magnitude as the partial molar volumes for H_2O_2 and OH.

Having determined the reaction volume, we can now quantify the density dependence of the equilibrium constant by integrating eq 3. We used the trapezoid rule to do the integration and

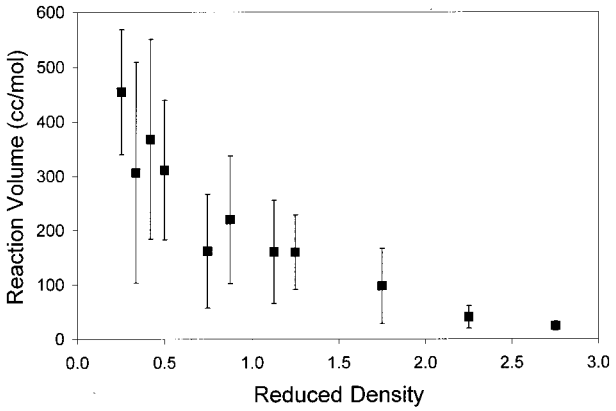

Figure 13. Reaction volume for H_2O_2 dissociation in SCW at $T_r = 1.15$.

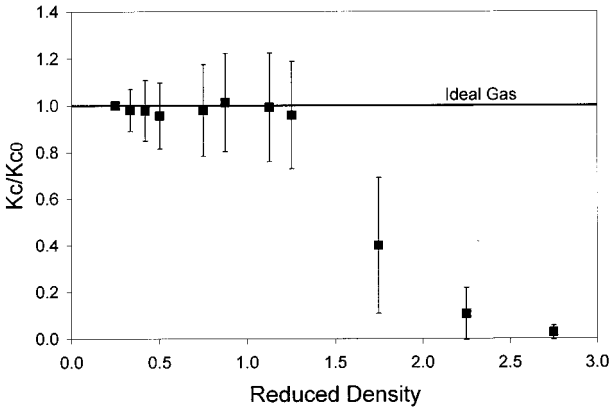

Figure 14. Relative equilibrium constants for H_2O_2 dissociation in SCW at $T_r = 1.15$. (■) Mean values from simulation and (−) ideal gas case.

thereby determine relative values of the equilibrium constant at various water densities. Figure 14 displays these relative equilibrium constants. The lowest density state was arbitrarily chosen as the reference point ($K_{c,0}$). Figure 14 shows that the equilibrium constant for H_2O_2 dissociation is a function of the water density. The mean value of the equilibrium constant (filled squares in Figure 14) changes by less than 5% between $0.25 < \rho_r < 1$, but it decreases by an order of magnitude as the reduced density continues to increase to 2.75. Note that this density dependence for the equilibrium constant arises from both the solute−solvent interactions (reaction volume) and the bulk solvent properties (density and isothermal compressibility − see eq 3). We speculate that the effects due to solute−solvent interactions dominate at low densities, while the effects due to bulk solvent properties dominate at high densities.

Figure 14 also displays the effect of the fluid density on the relative equilibrium constant for H_2O_2 dissociation in an ideal gas. In this case there is no density dependence.[62,63] We compare the simulation results to the ideal gas system because thermodynamic nonidealities are typically ignored when calculating the equilibrium constants used in mechanism-based modeling of SCWO kinetics. The equilibrium constants are then used to calculate the reverse rate constants. Assuming ideal-gas behavior (i.e. fugacity coefficients equal to unity) in detailed chemical kinetics models of SCWO is a practical necessity. The only current alternatives are to use a cubic equation of state with assumed critical constants for free radicals,[63] which is convenient but not very accurate,[30] or to use a molecular simulation approach as outlined here and by Mizan et al..[30] Our results show that the ideal-gas approximation may be adequate for H_2O_2 dissociation at low densities ($\rho_r < \sim 1.25$) at $T_r = 1.15$, although this conclusion must be tempered by a recognition of the uncertainties in the calculated equilibrium constants.

We have demonstrated that molecular simulation can be used to determine the effect of water density on an equilibrium constant at $T_r = 1.15$. A much larger number of state points need to be examined to develop a database sufficiently large to be useful in detailed chemical kinetics models of SCWO.

4. Conclusion

We have elucidated the water density effects on the reaction equilibrium constant for H_2O_2 dissociation in SCW at $T_r = 1.15$ and $\rho_r = 0.25-2.75$. We calculated the reaction volume from partial molar volumes for H_2O_2 and OH obtained from molecular dynamics simulations and Kirkwood−Buff theory. Both partial molar volumes and reaction volumes decreased monotonically with increasing water density. We used the reaction volume to quantify the water density dependence of the equilibrium constant for H_2O_2 dissociation in SCW. The mean value of the equilibrium constant for H_2O_2 dissociation changes by less than 5% between $0.25 < \rho_r < 1$, but it decreases by an order of magnitude between $1 < \rho_r < 2.75$.

From this study arises a systematic approach for improving the input parameters used in mechanism-based kinetics models of SCWO. One can first perform sensitivity analyses on the kinetics models to identify key elementary reaction steps in the overall reaction mechanism. Then, water density effects on the equilibrium constants, which are essentially manifestation of thermodynamic nonidealities, can be determined by the approach demonstrated in this study. The computational method is not limited to molecular dynamics simulation. Monte Carlo simulation and integral equation approaches are equally applicable, since only pair correlation functions are required.

A natural extension of this work is to determine activation volumes from simulation and use them to determine the density dependence of the rate constants. We discuss this extension in the following paper.

Acknowledgment. This material is based upon work supported by the National Science Foundation under Grants CTS-9521698 and CTS-9903373 and the Graduate Fellowship. N. A. thanks Prof. Robert Ziff and Kenneth Benjamin for helpful discussions and Javier Takimoto for technical assistance.

References and Notes

(1) Savage, P. E. *Chem. Rev.* **1999**, *99*, 603.
(2) Savage, P. E.; Gopalan, S.; Mizan, T. I.; Martino, C. J.; Brock, E. E. *AIChE J.* **1995**, *41*, 1723.
(3) Koo, M.; Lee, W. K.; Lee, C. H. *Chem. Eng. Sci*. **1997**, *52*, 1201.
(4) Holgate, H. R.; Tester, J. W. *J. Phys. Chem.* **1994**, *98*, 800.
(5) Thornton, T. D.; Savage, P. E. *AIChE J.* **1992**, *38*, 321.
(6) Oshima, Y.; Hori, K.; Toda, M.; Chommanad, T.; Koda, S. *J. Supercrit. Fluids* **1998**, *13*, 241.
(7) Steeper, R. R.; Rice, S. F.; Kennedy, I. M.; Aiken, J. D. *J. Phys. Chem.* **1996**, *100*, 184.
(8) Dell'Orco, P.; Foy, B.; Wilmanns, E.; Le, L.; Ely, J.; Patterson, K.; Buelow, S. In *Innovations in Supercritical Fluids: Science and Technology*; Hutchenson, K. W., Foster, N. R., Eds.; ACS Symposium Series 608; American Chemical Society: Washington, DC, 1995.
(9) Lee, D. S.; Park, K. S.; Nam, Y. W.; Kim, Y. C.; Lee, C. H. *J. Hazard. Mater.* **1997**, *56*, 247.
(10) Chang, K. C.; Li, L. X.; Gloyna, E. F. *J. Hazard. Mater.* **1993**, *33*, 51.
(11) Hamman, S. D. In *High-Pressure Physics and Chemistry*; Bradley, R. S., Ed.; Academic Press: London, 1963.
(12) Peck, D. G.; Mehta, A. J.; Johnston, K. P. *J. Phys. Chem.* **1989**, *93*, 4297.
(13) Kimura, Y.; Yoshimura, Y. *J. Chem. Phys.* **1992**, *96*, 3085.
(14) Kimura, Y.; Yoshimura, Y. *J. Chem. Phys.* **1992**, *96*, 3824.

(15) Kimura, Y.; Yoshimura, Y.; Nakahara, M. *J. Chem. Phys.* **1989**, *90*, 5679.
(16) Kirkwood, J. G.; Buff, F. P. *J. Chem. Phys.* **1951**, *19*, 774.
(17) Chialvo, A. A.; Cummings, P. T. *AIChE J.* **1994**, *40*, 1558.
(18) Chialvo, A. A. *J. Phys. Chem.* **1993**, *97*, 2740.
(19) Cummings, P. T.; Chialvo, A. A.; Cochran, H. D. *Chem. Eng. Sci.* **1994**, *49*, 1735.
(20) Debenedetti, P. G. *Chem. Eng. Sci.* **1987**, *42*, 2203.
(21) Tucker, S. C.; Maddox, M. W. *J. Phys. Chem. B* **1998**, *102*, 2437.
(22) Brock, E. E.; Savage, P. E.; Barker, J. R. *Chem. Eng. Sci.* **1998**, *53*, 857.
(23) Brock, E. E.; Oshima, Y.; Savage, P. E.; Barker, J. R. *J. Phys. Chem.* **1996**, *100*, 15834.
(24) Brock, E. E.; Savage, P. E. *AIChE J.* **1995**, *41*, 1874.
(25) Phenix, B. D.; Dinaro, J. L.; Tatang, M. A.; Tester, J. F.; Howard, J. B.; McRae, G. J. *Combust. Flame* **1998**, *112*, 132.
(26) Croiset, E.; Rice, S. F.; Hanush, R. G. *AIChE J.* **1997**, *43*, 2343.
(27) Teleman, O.; Jönsson, B.; Engström, S. *Mol. Phys.* **1987**, *60*, 193.
(28) Berendsen, H. J. C.; Postma, J. P. M.; van Gunsteren, W. F.; Hermans, J. In *Intermolecular Forces*; Pullman, B., Ed.; D. Reidel Publishing: Dordrecht, Netherlands, 1981.
(29) Mizan, T. I.; Savage, P. E.; Ziff, R. M. *J. Supercrit. Fluids* **1997**, *10*, 119.
(30) Mizan, T. I.; Savage, P. E.; Ziff, R. M. *AIChE J.* **1997**, *43*, 1287.
(31) Mizan, T. I.; Savage, P. E.; Ziff, R. M. *J. Comput. Chem.* **1996**, *17*, 1757.
(32) Mizan, T. I.; Savage, P. E.; Ziff, R. M. *J. Phys. Chem.* **1996**, *100*, 403.
(33) Mizan, T. I.; Savage, P. E.; Ziff, R. M. In *Innovations in Supercritical Fluids: Science and Technology*; Hutchenson, K. W., Foster, N. R., Eds.; ACS Symposium Series 608; American Chemical Society: Washington, DC, 1995.
(34) Mizan, T. I.; Savage, P. E.; Ziff, R. M. *J. Phys. Chem.* **1994**, *98*, 13067.
(35) Becke, A. D. *J. Chem. Phys.* **1993**, *98*, 5648.
(36) Miehlich, B.; Savin, A.; Stoll, H.; Preuss, H. *Chem. Phys. Lett.* **1989**, *157*, 200.
(37) Lee, C. T.; Yang, W. T.; Parr, R. G. *Phys. Rev. B.* **1988**, *37*, 785.
(38) Dobado, J. A.; Molina, J. M. *J. Phys. Chem.* **1993**, *97*, 7499.
(39) Chung-Phillips, A.; Jebber, K. A. *J. Chem. Phys.* **1995**, *102*, 7080.
(40) Gonzàlez, L.; Mò, O.; Yàñez, M. *J. Comput. Chem.* **1997**, *18*, 1124.
(41) Wang, B.; Hou, H.; Gu, Y. *Chem. Phys. Lett.* **1999**, *303*, 96.
(42) Boys, S. F.; Bernardi, F. *Mol. Phys.* **1970**, *19*, 553.
(43) Breneman, C. M.; Wiberg, K. B. *J. Comput. Chem.* **1990**, *11*, 361.
(44) Frisch, M. J.; Trucks, G. W.; Schlegel, H. B.; Gill, P. M. W.; Johnson, B. G.; Robb, M. A.; Cheeseman, J. R.; Keith, T.; Petersson, G. A.; Montgomery, J. A.; Raghavachari, K.; Al-Laham, M. A.; Zakrzewski, V. G.; Ortiz, J. V.; Foresman, J. B.; Peng, C. Y.; Ayala, P. Y.; Chen, W.; Wong, M. W.; Andres, J. L.; Replogle, E. S.; Gomperts, R.; Martin, R. L.; Fox, D. J.; Binkley, J. S.; Defrees, D. J.; Baker, J.; Stewart, J. P.; Head-Gordon, M.; Gonzalez, C.; Pople, J. A. *Gaussian94*, Revision B.3; Gaussian: Pittsburgh, 1995.
(45) Jorgensen, W. L. *J. Am. Chem. Soc.* **1979**, *101*, 2011.
(46) Press, W. H.; Teukolsky, S. A.; Vetterling, W. T.; Flannery, B. P. *Numerical Recipes in C: The Art of Scientific Computing*, 2nd ed.; Cambridge University Press: Cambridge, 1992; Chapter 7.
(47) Swaminathan, S.; Whitehead, R. J.; Guth, E.; Beveridge, D. L. *J. Am. Chem. Soc.* **1977**, *99*, 7817.
(48) Getino, C.; Sumpter, B. G.; Santamaria, J. *Chem. Phys.* **1990**, *145*, 1.
(49) Getino, C.; Sumpter, B. G.; Santamaria, J.; Ezra, G. S. *J. Phys. Chem.* **1990**, *94*, 3995.
(50) Martyna, G. J.; Tuckerman, M. E.; Tobias, D. J.; Klein, M. L. *Mol. Phys.* **1996**, *87*, 1117.
(51) Tuckerman, M.; Berne, B. J.; Martyna, G. J. *J. Chem. Phys.* **1992**, *97*, 1990.
(52) Hoover, W. G. *Phys. Rev. A* **1985**, *31*, 1695.
(53) Nosè, S. *Mol. Phys.* **1984**, *52*, 255.
(54) Allen, M. P.; Tildesley, D. J. *Computer Simulation of Liquids*; Oxford University Press: Oxford, 1987.
(55) Haile, J. M. *Molecular Dynamics Simulation: Elementary Methods*; John Wiley and Sons: New York, 1992.
(56) Neumann, M. *J. Chem. Phys.* **1985**, *82*, 5663.
(57) Cochran, H. D.; Cummings, P. T.; Karaboni, S. *Fluid Phase Equilib.* **1992**, *71*, 1.
(58) Cummings, P. T.; Cochran, H. D.; Simonson, J. M.; Mesmer, R. E.; Karaboni, S. *J. Chem. Phys.* **1991**, *94*, 5606.
(59) Petsche, I. B.; Debenedetti, P. G. *J. Chem. Phys.* **1989**, *91*, 7075.
(60) Debenedetti, P. G.; Mohamed, R. S. *J. Chem. Phys.* **1989**, *90*, 4528.
(61) Eckert, C. A.; Ziger, D. H.; Johnston, K. P.; Kim, S. *J. Phys. Chem.* **1986**, *90*, 2738.
(62) Sandler, S. T. *Chemical and Engineering Thermodynamics*; John Wiley and Sons: New York, 1989.
(63) Schmitt, R. G.; Butler, P. B.; French, N. B. *CHEMKIN Real Gas*; UIME PBB 93-066; Sandia National Laboratories: Albuquerque, 1994.